https://doi.org/10.2352/ISSN.2470-1173.2019.15.AVM-027

Signal Detection Theory and Automotive Imaging

Paul J. Kane; ON Semiconductor; Rochester, New York, USA

Abstract

Image quality (IQ) metrics are used to assess the quality of a detected image under a specified set of capture and display conditions. A large volume of work on IQ metrics has considered the quality of the image from an aesthetic point of view – visual perception and appreciation of the final result. Metrics have also been developed for "informational" applications such as medical imaging, aerospace and military systems, scientific imaging and industrial imaging. In these applications the criteria for image quality are based on information content and the ability to detect, identify and recognize objects from a captured image. Development of automotive imaging systems requires IQ metrics that are useful in automotive imaging. Many of the metrics developed for informational imaging are also potentially useful in automotive imaging, since many of the tasks – for example object detection and identification – are similar. In this paper, we review the Signal to Noise Ratio of the Ideal Observer and present it as a useful metric for determining whether an object can be detected with confidence, given the characteristics of an automotive imaging system. We also show how this metric can be used to optimize system parameters for a defined task.

Introduction

IQ metrics aimed at visual perception of the final image are appropriate for applications such as consumer photography with traditional cameras or cell phones, professional portraits, journalism and art. Metrics have also been developed for "informational" applications such as medical imaging, aerospace and military systems, scientific imaging and industrial imaging. In these applications the criteria for image quality are based on information content and the ability to detect, identify and recognize objects from a captured image. Specifications for these systems are developed based on the ability of an observer to use the system to reliably complete a task. In the age of increasingly automated automobiles, many of the metrics developed for informational imaging are applicable to automotive imaging, since many of the tasks – for example object detection and identification – are similar.

The development of sophisticated algorithms for detection, recognition and classification of objects in digital images has inspired the goal of replacing the human as the decision maker at the end of an imaging system. Whether or not this goal is achieved in any given application or at any point in time, the ability of an imaging system to enable a given task is still bounded by the laws of physics, and therefore it is still relevant to understand how these limits apply to the detected image. The performance of any observer or algorithm is limited by the information available in the input data. For example, in radiography, a large body of work has addressed the question of how imaging system characteristics affect the probability that an observer can correctly identify features in the image, leading to a successful diagnosis. In this paper, we show how this work can be applied to automotive imaging problems.

Signal Detection Theory

All captured images arise from the collection of photons, which give rise to photoelectrons at each collection site, or pixel. It is well known that the number of photoelectrons collected at each pixel is a Poisson random variable, whose distribution depends on the radiometric flux, the quantum efficiency of the sensor, the area of the pixel and the integration time. Early in the development of electronic imaging systems such as television, the random nature of image signals and its impact on the clarity of images was appreciated. Furthermore, it was recognized that the ability of an imaging system to detect an object depended on the contrast of the object against the background, the illumination level, and the spatial resolution of the detector. The inherent tradeoff between the collection area of each pixel (a larger area yielding a higher signal-to-noise ratio, or SNR) and the need for sufficient pixel density (pixels per unit area) to resolve small object features was also recognized. The early work of Rose [1] applied probability theory to calculate the minimum number of photons required to detect a pattern, with a set criterion for the maximum allowable number of "false alarms". A "false alarm" in signal detection theory means that the detected image is classified as belonging to an object of interest, when in fact the detected image has arisen entirely from random noise fluctuations. Clearly, as the image illumination and SNR increase, the probability of false alarms decreases. At the same time Rose was investigating the random nature of images, Schade [2] and others were investigating the application of linear systems theory to imaging systems. The concept of modulation transfer function was introduced to describe the effect of blur on images, and to identify the roles played by lenses and detectors in contributing to image blur. This work established a comprehensive model for image formation that included the linear systems treatment of image signal fidelity, image noise and the quantum nature of the detected signal that quantified the absolute performance of imaging systems. This is embodied in the concepts of Detective Quantum Efficiency (DQE) and Noise Equivalent Quanta (NEQ) [3]. The DQE and NEQ formalisms are used to great advantage in the analysis of radiographic imaging systems, in which the detection of weak signals is required. Extensions of the analysis demonstrate how quantities such as NEQ can be used to make statistical inferences of object detectability, given a set of system characteristics and scene conditions. This work is summarized in a well-known report [4], and is the starting point for our analysis.

The Ideal Observer

Inherent to the prediction of object detection and object discrimination are the concepts of task and observer. Examples of tasks are: Determining, to a specified degree of precision (1)

whether an object is present in an image or (2) whether an image area contains one, or two objects. The success of a task is measured in terms of how often the decision is made that an object is present, when the object is in fact present (true positive fraction or TPF), versus how often the decision is made that an object is present, when the object is not in fact present (false positive fraction or FPF). A plot of TPF vs. FPF, as a function of the decision criterion used, is called the Receiver Operating Characteristic (ROC) curve. The goal of system design is to maximize the TPF and minimize the FPF for the required tasks, which is equivalent to maximizing the area under the ROC curve [5].

The success of a task depends on the quality of the image and the behavior of the observer. Here "observer" is understood to mean a set of statistical decision criteria that model the performance of a human or algorithm. In order to establish the limits of detectability, we choose the best possible observer, that is, the observer that maximizes the statistical precision of the decision. In this way, we model the best possible outcome from a "perfect" human or algorithm, given the available image data. This ideal observer is a Bayesian decision maker who minimizes risk when selecting a decision criterion. This can be expressed in terms of a hypothesis test where two possible outcomes are, for example, H_1 (object is present) and H_2 (object is not present) when given an image $g(x,y)$, stated formally as follows [4]:

$$p(H_k \mid g(x,y)) = \frac{p(g(x,y) \mid H_k)\, p(H_k)}{p(g(x,y))} \tag{1}$$

where $p(a|b)$ is the conditional probability of a occuring given b, and $p(a)$ is the probability of a occurring. If we take the ratio for the two alternate hypotheses, we obtain the likelihood ratio L as follows:

$$L = \frac{p(g(x,y) \mid H_2)}{p(g(x,y) \mid H_1)} \tag{2}$$

This is the ratio of the probability of image $g(x,y)$ occuring, given that H_2 is true, to the probability of image $g(x,y)$ occuring, given that H_1 is true. The ideal observer compares the ratio L to a decision criterion C, and decides that H_2 is true if L is above C, and that H_1 is true if L is below C. The variable L has a distribution associated with each hypothesis, and the overlap of these distributions determines how successfully the two hypotheses can be separated. This is shown schematically in Fig. 1. The means of H_1 and H_2 are separated by a distance d', which is measured in units of standard devations. The distance d' is referred to as the Detectability Index. The larger the value of d', the better the separation between the two hypotheses, and the lower the FPF.

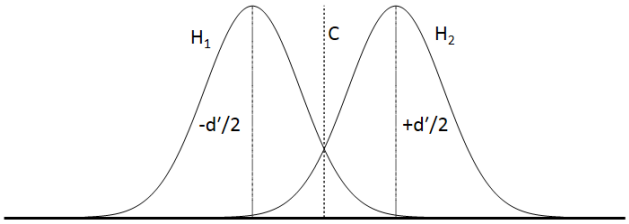

Figure 1. One possible distribution of L under hypotheses H1 and H2, showing decision criterion C and distance d'.

Figure of Merit for Task Performance

The performance of the Ideal Observer is quantified in terms of the Ideal Observer SNR, or *SNRI*. In the case where both the signal and the background are known exactly (SKE/BKE), the only random fluctuations in the image are due to noise, and it can be shown that *SNRI* is related to the imaging system characteristics as follows [4]:

$$SNRI^2 = K^2 \int \frac{|G(\nu)|^2\, MTF_{sys}^2(\nu)}{NPS(\nu)}\, d\nu = (d')^2 \tag{3}$$

Here K is the large area signal transfer factor, $G(\nu)$ is the Fourier Transform of the *difference* object, $MTF_{sys}(\nu)$ is the Modulation Transfer Function of the imaging system, $NPS(\nu)$ is the Noise Power Spectrum, and ν is the spatial frequency. The spatial frequency is understood here to be a vector quantity, with the integration performed in appropriate coordinates. By difference object, we mean the difference between the signals (objects) input to the system under the two hypotheses being tested. For object detection, this is the difference between the object and a uniform background (object not present). Equation (3) is a remarkable result, in that it permits us to determine the probability that the Ideal Observer chooses correctly between two hypotheses, given the Fourier spectra of the objects, the system MTF, and the NPS. We emphasize here that *SNRI* is the *signal-to-noise ratio of the decision made by the Ideal Observer, engaged in the specified task*, which in turn is based on the *frequency-dependent SNR of the imaging system.*

System Model

Computation of *SNRI* requires calculation of the capture system MTF, the image noise and a model for the difference object. The *SNRI* and the quantities that it depends upon are channel-dependent, meaning that we calculate a separate *SNRI* for each color channel in the system. The quantities inside the integral must be weighted by the spectral response of the channel, if they are known as a function of wavelength, or measured directly with the appropriate spectral weighting. For example, in the case of an RGB sensor, we would calculate *SNRI* values for each of the red, green and blue color images detected by the sensor. If the detected signals are combined, for example into luminance and chrominance (color-difference) signals, we can compute *SNRI* values for these combinations.

We follow the model proposed by Jenkin and Kane [6], beginning with the system MTF, which includes contributions

from the lens, pixel, demosaic algorithm, and crosstalk. For color channel *k* we have:

$$MTF_{sys,k}(\nu) = MTF_{lens,k}(\nu) \cdot MTF_{pixel,k}(\nu) \cdot MTF_{dem,k}(\nu) \cdot MTF_{cross,k}(\nu) \tag{4}$$

The lens MTF can be determined from the usual diffraction-limited formula [7], from design data or from laboratory measurements. As an example of spectral weighting for channel-dependent quantities, the lens MTF for channel *k* may be determined from the wavelength-dependent lens MTF as follows:

$$MTF_{lens,k}(\nu) = \frac{\int MTF_{lens}(\nu,\lambda) QE_k(\lambda) d\lambda}{\int QE_k(\lambda) d\lambda} \tag{5}$$

Here $QE_k(\lambda)$ is the quantum efficiency of the *k*th channel, and λ is the wavelength. The pixel MTF is usually determined on a per-channel basis. An ideal, channel-independent pixel MTF may also be used:

$$MTF_{pixel,k}(\nu) = \frac{\sin(\pi p \nu)}{\pi p \nu} \tag{6}$$

where *p* is the pixel width. A more realistic model includes the phase differences between the image and the sampling grid [6]. The average pixel response including this factor may be written:

$$MTF_{pixel,k}(\nu) = \frac{\cos^2(\pi s \nu)\sin(\pi p \nu)}{\pi p \nu}, \tag{7}$$

where *s* is the sampling pitch.

The demosaic MTF depends on the layout and relative proportions of the colored pixels [8]. For example, in the Bayer pattern, the green channel has a broader MTF than the other channels since there are twice as many green pixels as red or blue. Note that the component MTFs do not necessarily have polar symmetry, so this must be accounted for when applying Eq. (3). Any additional blurring effects, such as atmospheric degradation, windscreen effects or motion blur can also be included in Eq. (4).

We also need a model for the photoelectron signal in each channel, in particular so that we can determine the NPS, which is signal-dependent. The model should include the spectral characteristics of the object (including illumination), the quantum efficiency of the channel, and the radiometric characteristics of the capture system. Again following Jenkin and Kane [6], the number of photons detected by a pixel during integration time T_{INT} is given by:

$$PH_{pixel} = \int \frac{h \cdot c \cdot T_{INT} P_{PIXEL}(\lambda)}{\lambda} d\lambda, \tag{8}$$

where *h* is Planck's constant, *c* is the speed of light, and $P_{pixel}(\lambda)$ is the detected power per wavelength per pixel. The latter quantity is given by:

$$P_{pixel}(\lambda) = I(\lambda) \cdot F(\lambda) \cdot QE(\lambda) \cdot \Omega \cdot A_{pixel}, \tag{9}$$

where $I(\lambda)$ is the illumination in W/nm/pixel at the sensor, $F(\lambda)$ is the spectral response of the optics including any IR filters, $QE(\lambda)$ is the quantum efficiency as before, and A_{pixel} is the area of a pixel. The radiometric efficiency Ω is given by:

$$\Omega = \frac{\pi\tau}{4N^2}, \tag{10}$$

where τ is the transmission factor of the optics and *N* is the f-number of the optical system.

For the noise model, we assume that the NPS is flat, and therefore this term in Eq. (3) can be replaced by the noise variance, if the integration of Eq. (3) is performed in cycles/pixel [9]. The total noise variance is a sum of the variances of the independent noise sources in the sensor. We include signal-dependent photon shot noise and photo response non-uniformity (PRNU), and signal-independent read noise and dark signal non-uniformity (DSNU). The latter is the residual random noise after dark current correction. The total noise variance is given by:

$$\sigma_N^2 = \overline{Q} + (\overline{Q} \cdot \sigma_{PRNU})^2 + \sigma_{RN}^2 + \sigma_{DSNU}^2, \tag{11}$$

where σ_N is the total RMS noise, $\overline{Q}$ is the mean signal in photoelectrons, σ_{RN} is the read noise, σ_{PRNU} is the PRNU noise, and σ_{DSNU} is the DSNU noise. Here we have used the fact that for photon shot noise, the variance is equal to the mean signal level. In general, each of these terms will be channel-dependent. Linear combinations of individual channel outputs (for example, luma/chroma signals, color correction operations) can be modeled using linear algebra, with standard equations for propagation of MTF and NPS through matrix operations [10].

Object Detection

Detecting objects on the road is critical to safe driving. When approaching an object on the road, the driver must decide whether an evasive maneuver should be undertaken. An example problem is a cobblestone-like object, with a 15cm square cross section, at a distance of 150m under headlight illumination, and a specified contrast relative to the background. Figure 2 represents the profile of such an object in terms of its offset ΔQ above a background photon flux $\overline{Q}$. The object has a width *w*, an area $A=w^2$ and a contrast $C = \Delta Q/\overline{Q}$. For the problem of detecting the object against the background, the difference object is modeled as follows:

$$\Delta g(x,y) = \Delta Q \cdot rect\,(x/w) \cdot rect(y/w) \tag{12}$$

where the function *rect(x/w)* has value 1 when $x < w$, 1/2 when $x = w$ and zero when $x > w$. The Fourier Transform of this function is:

$$G(\nu_x,\nu_y) = w^2 \cdot \Delta Q \cdot \frac{\sin(\pi w \nu_x)}{\pi w \nu_x} \cdot \frac{\sin(\pi w \nu_y)}{\pi w \nu_y} \tag{13}$$

where ν_x, ν_y are spatial frequencies in the *x* and *y* directions. Substituting into Eq. (3), assuming that the only source of noise is spatially uncorrelated photon shot noise, and that the system MTF is approximately unity over the spatial frequency range of interest, we obtain the following result:

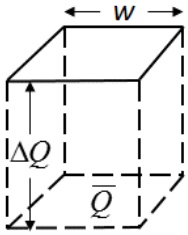

Figure 2. Model of a square object of contrast $C = \Delta Q / \overline{Q}$ *and width w.*

$$SNRI = C \cdot \sqrt{\overline{Q} A} \tag{14}$$

Equation (14) is the result expected from a first-order analysis of signal to noise, neglecting system blur. Figure 3 shows four simulated images of square objects illustrating the interpretation of Eq. (14). With the photon flux held constant, the contrast *C* and area *A* of the objects are varied, resulting in a constant value of *SNRI*. As the object area increases, more detection events at the sensor means that a lower object contrast is required to produce the same statistical confidence of detection (*SNRI)*. This simple relationship holds for quantum limited detection when the blur of the system is negligible. When the width of the system point spread function is on the order of the object size, the integral of Eq. (3) must be evaluated.

Object Detection with Varying Illumination and Distance

We now consider a full application of Eq. (3) and Eq. (13) for the cobblestone object described in the previous section. The parameters of the simulated lens and sensor are shown in Table 1. The goal is to determine the dependence of *SNRI* on object distance under automotive headlight illumination that decreases over distance. The illuminance falloff is derived from a fit to published data [11] on automotive headlight characteristics. These data are well fit by the simple model $I = 26000/D^2$, where *D* is the distance in meters and *I* is the illuminance in lux. The spectrum of the illuminant is that of a white LED headlight, measured in the laboratory.

In this example, a camera system with a 30 degree field of view (FOV) and a sensor 3840 pixels/column x 2.1 μm/pixel = 8mm wide requires a 15mm focal length lens, leading to a magnification of 10^{-4} for an object at 150m, implying an image just over 7 pixels on a side. Intuitively this seems like enough pixels to detect that something is there, but the object contrast, illumination and system MTF must also be considered. We use a diffraction-limited lens MTF model, weighted by the sensor QE as shown in Eq. (5), and the ideal pixel MTF shown in Eq. (7). We compute the *SNRI* for two cases, corresponding to QE curves for an RGB sensor and an RCB sensor (with the same R,B channels in both cases). Figure 4 shows these, as well as the spectrum of an LED headlamp, and the spectral transmittance of an IR cut filter with stop band beginning at approximately 670nm.

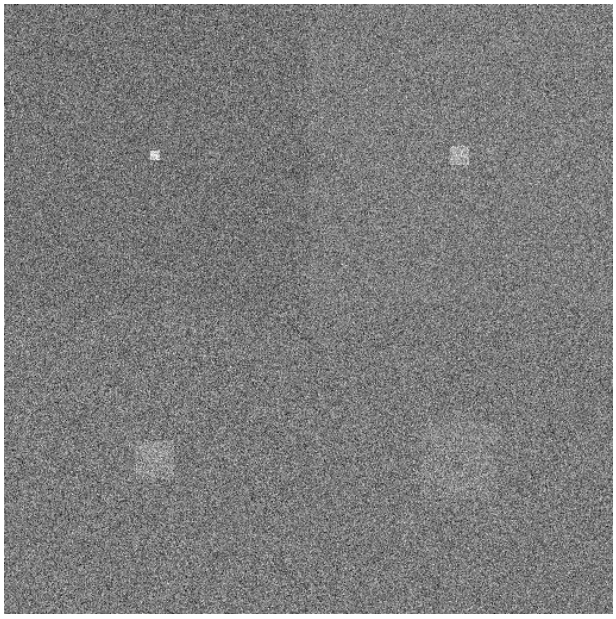

Figure 3. Simulated images of square objects of varying size and contrast with equal SNRI.

Object		**Sensor**		**Lens**	
Size (mm)	150	Pixel size (μm)	2.1	FOV (deg)	30
Distance (m)	50-200	Columns	3840	f/#	1.4
Contrast (%)	20	Read noise (e-)	2	IR cutoff (nm)	670
Headlamp spectrum	White LED	DSNU (e-)	4	Transmittance	0.9
		PRNU (%)	0.8	Focal length (mm)	15
		Int. time (msec)	10		

Table 1. Simulation inputs.

For object detection, we consider a comparison between a broadband image produced by a demosaic of the clear channel of the RCB sensor to full frame, and a weighted RGB (luma) channel from the RGB sensor, also assuming a demosaic of each channel, using typical RGB weighting coefficients of [0.299, 0.5870, 0.1140]. A distance range of 50 to 200m is considered.

We expect that the result from the clear channel image will have superior SNR to that of the weighted RGB, since the noise of the RGB channels, which are narrower in bandwidth compared to the clear, add in quadrature. In addition, the demosaic of the R and

B channels is inferior to that of the G or C, since they are sparser in the CFA pattern. Figure 5 demonstrates that this is the case.

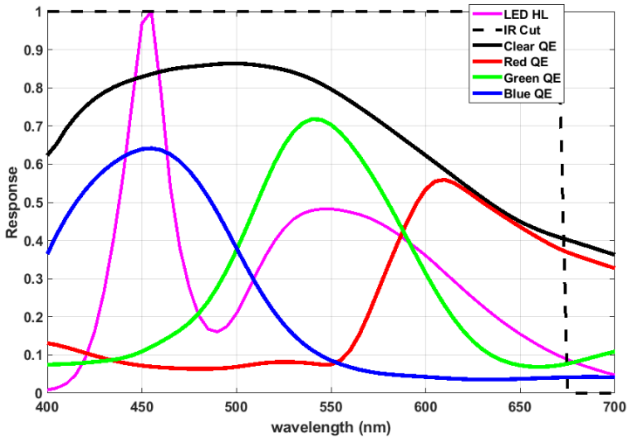

Figure 4. Spectral data.

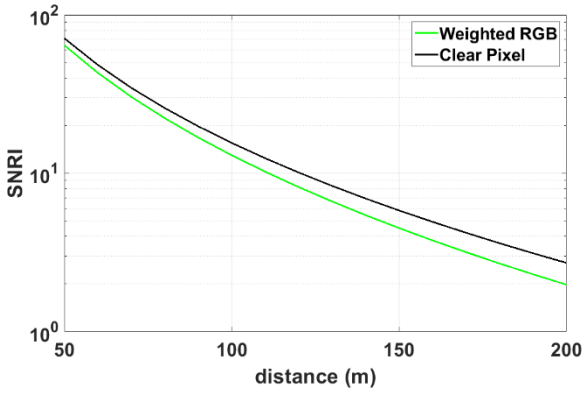

Figure 5. SNRI vs. object distance for clear and weighted RGB channels.

Figure 5 also shows the expected decrease of *SNRI* with distance, due to the falloff in headlamp illumination, the decrease in image size on the sensor, and the increasing impact of the system MTF. The separation between the weighted RGB and the clear channel increases slightly with distance, due to the difference in demosaic MTF just described.

Optimum Pixel Size

One question that frequently arises in selecting a sensor for an application is the choice of pixel size and number of pixels, or format. The latter is sometimes informally called "resolution", although "resolution" is a more complex metric of performance that includes MTF and noise. The fundamental tradeoff in pixel size is signal strength vs. pixel density at the object. Larger pixels capture more light and provide better signal to noise, at the expense of pixels per object. The *SNRI* metric can quantify this tradeoff for a given task, by repeating the *SNRI* vs. distance analysis at a series of pixel sizes. The system parameters are the same as in Table 1, except that we vary the pixel size and pixel number at fixed sensor size, as shown in Table 2.

Pixel size (μm)	1.05	2.1	4.2	8.4
Columns	7680	3840	1920	960
Object Area (pixels) at 150m	205	51	13	4

Table 2. Pixel size and sensor format.

Two cases are shown, both for the clear channel of an RCB sensor. In the first case, a noise floor of zero is assumed, so that the only noise in the image is due to photon shot noise, with the results shown in Fig. 6.

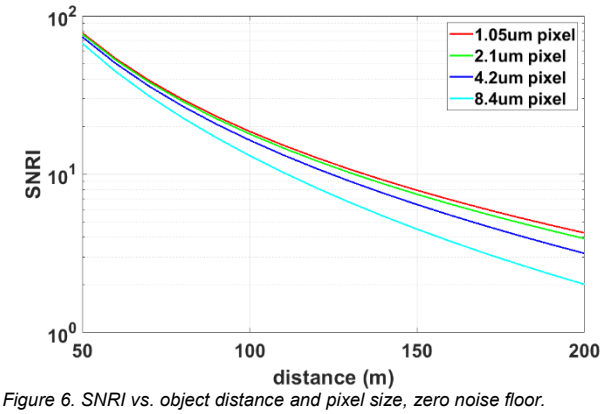

Figure 6. SNRI vs. object distance and pixel size, zero noise floor.

The three smaller pixel sizes are fairly similar in performance at short distances, when there object is larger and the illumination level is high. These begin to separate at larger distances, where a smaller pixel size in the same sensor format implies a larger number of pixels on the object. The 1.05 μm and 2.1μm pixel sizes are closer in performance at long distances. Even though the 2.1μm sensor has 4x less number of pixels, the larger pixel area provides more signal, which narrows the gap. Figure 7 shows the effect of adding a noise floor of approximately 3.5e-, which might arise from a combination of read noise and DSNU.

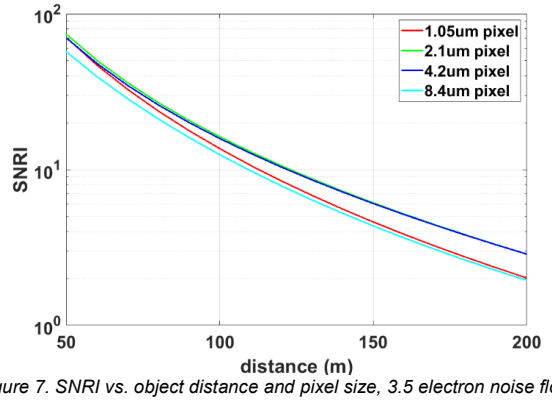

Figure 7. SNRI vs. object distance and pixel size, 3.5 electron noise floor.

The presence of the noise floor alters the tradeoff between radiometric efficiency (pixel area) and resolution (number of pixels). Now there appears to be an optimum pixel size in the range of 2.1μm to 4.2μm, with both the largest and smallest pixel sizes lagging in performance. This shows that there may be a range of pixel sizes that yield the highest *SNRI* for a particular task and sensor noise level. Note that we have assumed here that the signal-independent sensor noise and the QE are the same across all pixel sizes, which may not be true in practice. Also, only the task of object detection has been considered here. An automotive camera may need to be optimized for multiple tasks, leading to other tradeoffs.

Motion Detection

Another important task in automotive and security imaging is detecting moving objects. This is usually done by comparing the content of successive frames in a video sequence. Here we ask, what is the probability of detecting that an object of a certain size, at a certain distance and illumination level, has moved? Here the signal under consideration is the difference image between the two frames. If only one object has moved, the rest of the difference image is zero. For a linear translation of an object along the x axis, it can be shown [12] that the object spectrum of Eq. (13) is modified as follows:

$$\left|G(\nu_x,\nu_y)\right|^2 \rightarrow \left|G(\nu_x,\nu_y)\right|^2 \sin^2(\pi\cdot\Delta x\cdot\nu_x) \qquad (19)$$

where Δx is the object shift between frames in pixels, assuming the frequency axis is in cycles/pixel. The shift in pixels can be related to the translation of the object through the pixel size and the optical magnification. Figure 8a shows a plot of the function in Eq. (19) for the case of no shift ($\Delta x=0$). The spectrum has been normalized to 1.0 at maximum value.

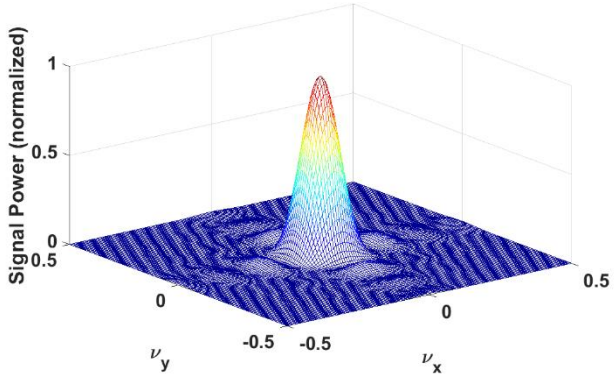

Figure 8a. Difference object spectrum for detection with a constant background.

Figure 8b shows the plot for the case of a one pixel shift ($\Delta x=1$). We see that for small shift values, the difference object spectrum shows significant high frequency content as compared to the original object detection task. As the shift increases, the size of the feature in the difference image increases, and the importance of the high spatial frequencies once again diminishes, eventually looking very similar to Fig. 8a. This makes sense in that at small shift values, the difference between frames is spread over a very small area. However, as the shift approaches the size of the object, the difference image is spread over a much larger area.

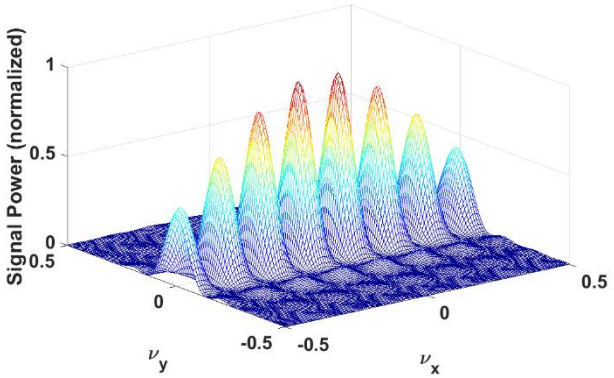

Figure 8b. Difference object spectrum for detection of object motion (one pixel translation of square object).

Figure 9 shows the *SNRI* plotted against the amount of object shift, here in terms of distance across the plane of the object, for several object sizes, at a fixed distance of 150m, once again analyzing the clear channel. We see that the *SNRI* value increases with object shift until it reaches a plateau as the shift exceeds the size of the object. We also see that the overall magnitude of *SNRI* increases with overall object size, which is expected since the size of the area in the difference image is larger. For the smaller objects, the probability of detecting object translation at this distance (150m) is very small compared to the largest object, for which shifts of a few pixels can be reliably detected.

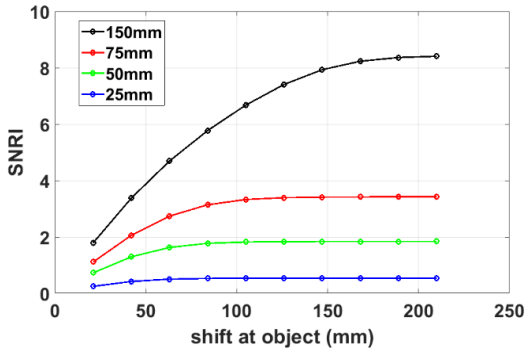

Figure 9. SNRI vs. object shift for several object sizes at 150m.

Summary

The detection of objects, object motion and other changes between image frames is limited by the physics of image capture, namely photon noise, electronic noise and image blur. Signal detection theory provides tools that can be used to establish the fundamental limits of detection for a given task. This analysis has proven useful in medical imaging, and we have shown that it can also be useful in automotive imaging. The performance of image processing algorithms and recognition tasks is necessarily limited by the

information content of the input image, which can be analyzed using these techniques.

Acknowledgements

This work was stimulated by discussions about object detection with my colleagues David Amey, Scott Johnson and James Tornes at ON Semiconductor, to whom I am very grateful.

References

[1] A. Rose, Vision: Human and Electronic: Plenum Press, 1973.

[2] O. Schade, "The resolving-power functions and quantum processes of television cameras", RCA Rev., vol. 28, pp. 460-535 1967.

[3] J. C. Dainty and R. Shaw, Image Science: Academic, 1974.

[4] ICRU Report 54, Medical Imaging – The Assessment of Image Quality, Bethesda MD: International Commission on Radiation Units and Measurements, 1996.

[5] D. M. Green and J. A. Swets, Signal Detection Theory and Psychophysics: Peninsula Publishing, 1966.

[6] R. Jenkin and P. Kane, "Fundamental Imaging System Analysis for Autonomous Vehicles", in Electronic Imaging: Autonomous Vehicles and Machines 2018, Burlingame, California, 2018.

[7] W. J. Smith, Modern Optical Engineering, Third Edition: SPIE Press, 2000.

[8] K. Topfer, J. E. Adams and B. W. Keelan, "Modulation Transfer Functions and Aliasing Patterns of CFA Interpolation Algorithms", in IS&T's 1998 PICS Conference, Portland, Oregon, 1998.

[9] B. W. Keelan, "Imaging Applications of Noise Equivalent Quanta", in Electronic Imaging: Image Quality and System Performance XIII Burlingame, California, 2016.

[10] B. W. Keelan, Handbook of Image Quality: Marcel Dekker, 2002.

[11] H. Joachim and Schmidt Clausen, "The Visibility Distance of a Car-Driver in Driving Situation", in SAE International Congress and Exposition, Society of Automotive Engineers, 1982.

[12] K. M. Hanson, "Variations in Task and the Ideal Observer", Proc. SPIE vol. 419, pp. 60-67, 1983.

Author Biography

Paul J. Kane received a B.S. in Physics from the University of Scranton and an M.S. in Optics from the University of Rochester. He was a scientist at the Kodak Research Laboratories for 28 years, working primarily in the areas of imaging science and optics. His projects there included system modeling and simulation, image processing for OLED displays, 3D imaging and light scattering from small particles. In 2015 he joined ON Semiconductor as an Algorithm Design Engineer, focusing on automotive and security applications. Mr. Kane holds 35 U.S. patents in the areas of algorithms, display technologies and solid state lighting. He is a Senior Member of SPIE.

JOIN US AT THE NEXT EI!

IS&T International Symposium on

Electronic Imaging

SCIENCE AND TECHNOLOGY

Imaging across applications . . . Where industry and academia meet!

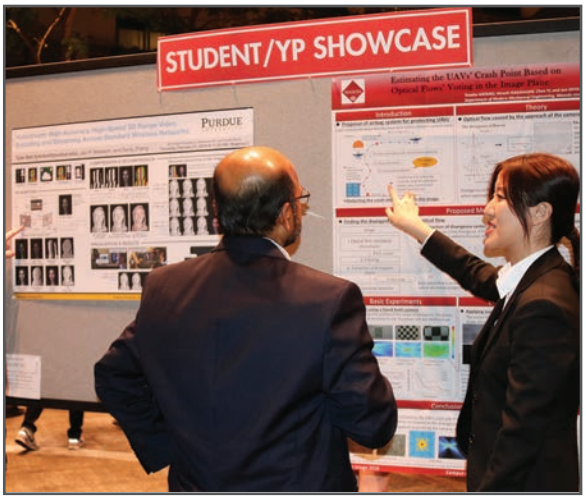

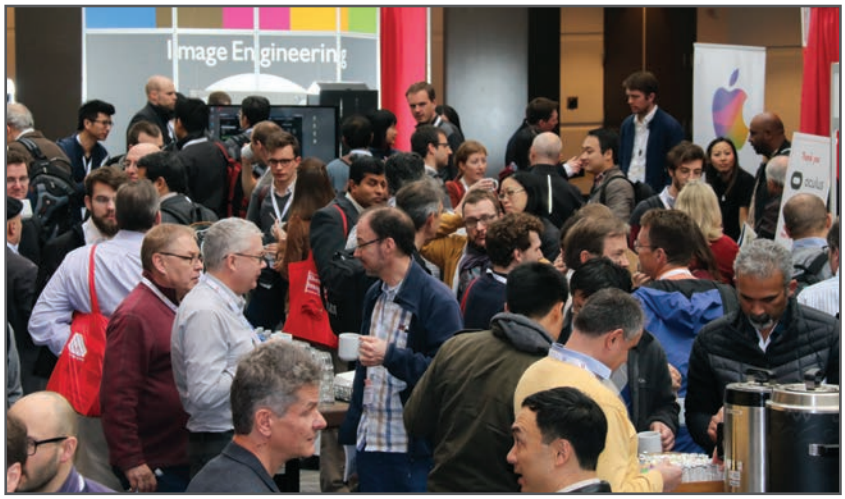

• SHORT COURSES • EXHIBITS • DEMONSTRATION SESSION • PLENARY TALKS •
• INTERACTIVE PAPER SESSION • SPECIAL EVENTS • TECHNICAL SESSIONS •

www.electronicimaging.org

IS&T
imaging.org